

# HIP 67506 C: MagAO-X Confirmation of a New Low-Mass Stellar Companion to HIP 67506 A

Logan A. Pearce<sup>1,2\*</sup>, Jared R. Males<sup>1</sup>, Sebastiaan Y. Haffert<sup>1,10</sup>, Laird M. Close<sup>1</sup>, Joseph D. Long<sup>1</sup>, Avalon L. McLeod<sup>1,3</sup>, Justin M. Knight<sup>1,3</sup>, Alexander D. Hedglen<sup>1,3</sup>, Alycia J. Weinberger<sup>4</sup>, Olivier Guyon<sup>1,3,5,6</sup>, Maggie Kautz<sup>1,3</sup>, Kyle Van Gorkom<sup>1,3</sup>, Jennifer Lumbres<sup>1,3</sup>, Lauren Schatz<sup>8</sup>, Alex Rodack<sup>1,3</sup>, Victor Gasho<sup>1</sup>, Jay Kueny<sup>1,3</sup>, Warren Foster<sup>1,3</sup>, Katie M. Morzinski<sup>1</sup>, Philip M. Hinz<sup>9</sup>

<sup>1</sup>Steward Observatory, University of Arizona, Tucson, AZ 85721, USA

<sup>2</sup>NSF Graduate Research Fellow

<sup>3</sup>James C. Wyant College of Optical Sciences, University of Arizona, 1630 E University Blvd, Tucson, AZ 85719, USA

<sup>4</sup>Earth and Planets Laboratory, Carnegie Institution for Science, 5241 Broad Branch Road NW, Washington, DC 20015-1305

<sup>5</sup>National Astronomical Observatory of Japan, Subaru Telescope, National Institutes of Natural Sciences, Hilo, HI 96720, USA

<sup>6</sup>Astrobiology Center, National Institutes of Natural Sciences, 2-21-1 Osawa, Mitaka, Tokyo, JAPAN

<sup>8</sup>Kirtland Air Force Base, Air Force Research Laboratory, Albuquerque, NM, USA

<sup>9</sup>UC Santa Cruz, 1156 High St, Santa Cruz CA 95064, USA

<sup>10</sup>NASA Hubble Fellow

Accepted XXX. Received YYY; in original form ZZZ

## ABSTRACT

We report the confirmation of HIP 67506 C, a new stellar companion to HIP 67506 A. We previously reported a candidate signal at  $2\lambda/D$  (240 mas) in  $L'$  in MagAO/Clio imaging using the binary differential imaging technique. Several additional indirect signals showed that the candidate signal merited follow-up: significant astrometric acceleration in Gaia DR3, Hipparcos-Gaia proper motion anomaly, and overluminosity compared to single main sequence stars. We confirmed the companion, HIP 67506 C, at 0.1" with MagAO-X in April, 2022. We characterized HIP 67506 C MagAO-X photometry and astrometry, and estimated spectral type K7-M2; we also re-evaluated HIP 67506 A in light of the close companion. Additionally we show that a previously identified 9" companion, HIP 67506 B, is a much further distant unassociated background star. We also discuss the utility of indirect signposts in identifying small inner working angle candidate companions.

**Key words:** planets and satellites: detection, (stars:) binaries: visual, stars: statistics, methods: data analysis, methods: observational

## 1 INTRODUCTION

High-contrast imaging searches have found very low occurrence rates for close substellar companions. For example,  $9^{+5}_{-4}\%$  for 5-13  $M_{\text{Jup}}$ ,  $\sim 0.8^{+0.8}_{-0.5}\%$  for 13-80  $M_{\text{Jup}}$  companions within 10-100 AU in the recent results from the Gemini Planet Imager Exoplanet Survey ( GPIES); (Nielsen et al. 2019), while the SHINE survey (Vigan et al. 2021) found frequency of systems with at least one substellar companion to be  $23.0^{+13.5}_{-9.7}\%$ ,  $5.8^{+4.7}_{-2.8}\%$ , and  $12.6^{+12.9}_{-7.1}\%$  for BA, FGK, and M stars. Yet radial velocity, transit, and microlensing surveys point to higher occurrence rates in regions promising for future direct imaging contrasts and separation (e.g. Bryan et al. 2019; Herman et al. 2019; Poleski et al. 2021). Decreasing the effective inner working angle (IWA) of observations increases the area of the accessible region proportional to  $(\text{IWA})^{-2}$ . Smaller IWAs extend the reach to tighter regimes of nearby stars, and to the planetary regime of more distant

stars (Mawet et al. 2012). Working at small IWAs will be vital for the future of the high-contrast imaging field.

Rodigas et al. 2015 demonstrated that for visual binaries of separation  $\approx 2 - 10''$  and approximately equal magnitude, a starlight subtraction via a principal component analysis-based reference differential imaging (RDI) algorithm using each star of the binary as reference for the other – termed binary differential imaging (BDI) – outperforms the common angular differential imaging technique at close separations. In Pearce et al. 2022 we used BDI to reduce a set of 17 visual binaries imaged in  $L'$  and  $3.95\mu\text{m}$  filters with MagAO/Clio instrument on the Magellan Clay Telescope at Las Campanas Observatory from 2015-2017. In that work we reported detection of a candidate companion signal at  $2\lambda/D$  separation to the star HIP 67506 A. Due to the proximity to the star's core we were unable to determine the nature of the companion, but had evidence to suggest it might be near the stellar/substellar mass boundary.

In this work we report the results of follow-up observations of HIP 67506 A with the MagAO-X instrument on the Magellan Clay

\* E-mail: loganpearce1@arizona.edu

telescope in April 2022 to confirm the candidate signal. We report the discovery of HIP 67506 C, a previously unknown early-M type  $0.1''$  ( $\sim 20$  AU) companion to HIP 67506 A. In Section 2 we describe the indirect indications pointing to the existence of a hidden companion. In Section 3 we describe our MagAO-X follow up observations and confirmation of HIP 67506 C, and in Section 4 our astrometric and photometric characterization. Additionally in Appendix A we demonstrate that the previously identified  $9''$ -separated star HIP 67506 B is not actually physically associated.

## 2 STELLAR PROPERTIES

HIP 67506 A is a field star (99.9% probability in BANYAN  $\Sigma$ ; Gagné et al. 2018) at  $221.6 \pm 1.8$  pc (Gaia Collaboration et al. 2021). It was identified as type G5 (Spencer Jones & Jackson 1939), mass  $1.2 M_{\odot}$  (Chandler et al. 2016), with effective temperature  $T_{\text{eff}} = 6077 \pm 150$  K and luminosity  $L = 0.37 \pm 0.07 L_{\odot}$  (McDonald et al. 2012). In Pearce et al. (2022) we used these values to estimate an age of  $\approx 200$  Myr from isochrone fitting to Baraffe et al. (2015) isochrones. It was identified in the Hipparcos and Tycho Doubles and Multiples Catalog (ESA 1997) as a binary system with another star (HIP 67506 B) with separation  $9''$ , and dubbed HIP 67506 A and B.

### 2.1 Indicators of a companion to HIP 67506 A

In Pearce et al. (2022) we observed 17 visual binary systems and reduced the images using the Binary Differential Imaging (BDI) technique (see also Rodigas et al. 2015) with Magellan Adaptive Optics system (MagAO) (Close et al. 2013) and Clio science camera on the Magellan Clay Telescope at Las Campanas Observatory in MKO  $L'$  and  $3.95\mu\text{m}$  filters, from 2014–2017. To summarize briefly, we simultaneously observed a science and PSF reference target by selecting binaries of nearly equal magnitude, separated enough that their PSF features do not overlap, but close enough to be within the isoplanatic patch at these wavelengths, making the target and reference PSF as close to equal in structure and signal-to-noise ratio as possible. We then reduced each star with the other as the PSF reference, using Karhunen-Loève Image Projection (KLIP; Soummer et al. 2012) to reconstruct a model PSF from the reference star to subtract from the target star.

We observed HIP 67506 AB on 2015-05-31 as part of this survey and detected a candidate companion signal  $\sim 0.2''$  East of HIP 67506 A. Figure 1 displays the KLIP-reduced image of HIP 67506 A from that paper, with the candidate signal marked by the red circle. The candidate signal is distorted from a typical PSF shape – due its proximity to the star’s core (at  $2\lambda/D$ ) the signal was corrupted by PSF subtraction. However the fact that it did not appear to smear azimuthally like the other residuals at that same separation points to the possibility of its being a true companion signal.

There are secondary indications of a companion to HIP 67506 A. Figure 2 shows a Gaia EDR3 BP minus RP vs absolute G magnitude color-magnitude diagram of Praesepe Cluster members identified in Deacon & Kraus 2020 (orange), reproducing their Figure 4. Members they flagged as overluminous and with elevated astrometric noise in Gaia EDR3, indicating an unresolved companion, are marked with blue and purple triangles respectively. HIP 67506 A is marked with a red star in the main and inset axes. HIP 67506 A clearly falls on the overluminous region above the main sequence, indicating that the flux measured by Gaia is abnormally high for a single star, pointing to the presence of an unresolved stellar companion.

HIP 67506 A also has indicators of an unresolved companion in

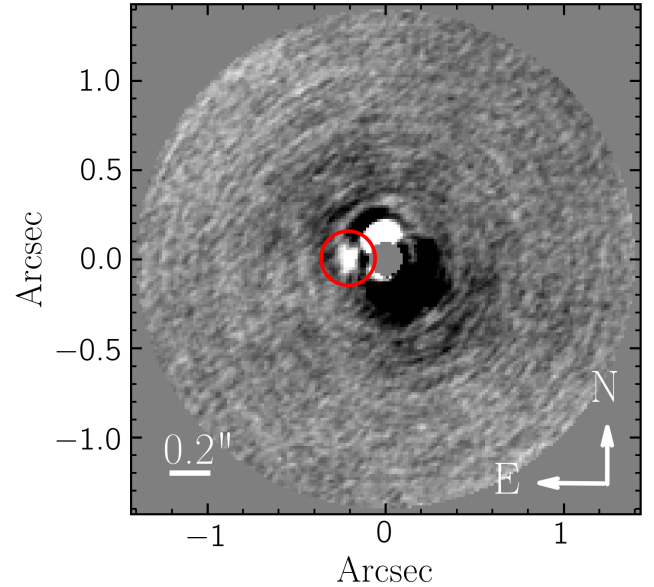


**Figure 1.** MKO  $L'$  KLIP-reduced image of HIP 67506 A from our Binary Differential Imaging survey described in Pearce et al. (2022). The central star is masked in the reduction, and the candidate signal is marked with a red circle  $\sim 2''$  ( $2.0 \lambda/D$ ) to the east. This was identified as a candidate signal due to the fact that it did not appear to smear azimuthally with derotation like the other residual structures at similar separation, and the other indications described in Section 2.1

Gaia astrometry. The Gaia Renormalized Unit Weight Error (RUWE) is a signpost for unresolved companions. RUWE encapsulates all sources of error in the fit to the assumed single star astrometric model, corrected for correlation with source color and magnitude.  $\text{RUWE} \approx 1$  is expected for a well-behaved solution (Lindgren 2018)<sup>1</sup>.  $\text{RUWE} > 2$  indicates significant deviation from a single star model. HIP 67506 A has  $\text{RUWE} = 2.02$  in Gaia EDR3, indicating that a companion is likely.

While RUWE is the most complete and easy to interpret metric (Lindgren 2018), other metrics in Gaia can probe multiplicity. Perturbations of the source photocenter (caused by orbiting unresolved objects) compared to the center-of-mass motion (which moves as a single star) will cause the observations to be a poor match to the fitting model, which registers as excess noise via the `astrometric_excess_noise` parameter, and whose significance is captured in the `astrometric_excess_noise_sig` parameter ( $> 2$  indicates significant excess noise). The `astrometric_chi2_all` term reports the  $\chi^2$  value of the observations to the fitting model, with lower values indicating better fit to observations. From the image parameter determination (IPD) phase, `ipd_gof_harmonic_amplitude` is sensitive to elongated PSF shapes relative to the scan direction (larger values indicate more elongation), and `ipd_frac_multi_peak` reports the percentage of observations which contained more than one peak in the windows<sup>2</sup>.

Table 1 shows values of these metrics for HIP 67506 A. The IPD parameters are small and insignificant, suggesting that there are no

<sup>1</sup> <https://www.cosmos.esa.int/web/gaia/dr2-known-issues#AstrometryConsiderations>

<sup>2</sup> See [https://gea.esac.esa.int/archive/documentation/GEDR3/Gaia\\_archive/chap\\_datamodel/sec\\_dm\\_main\\_tables/sssec\\_dm\\_gaia\\_source.html](https://gea.esac.esa.int/archive/documentation/GEDR3/Gaia_archive/chap_datamodel/sec_dm_main_tables/sssec_dm_gaia_source.html) for complete description of Gaia catalog contents

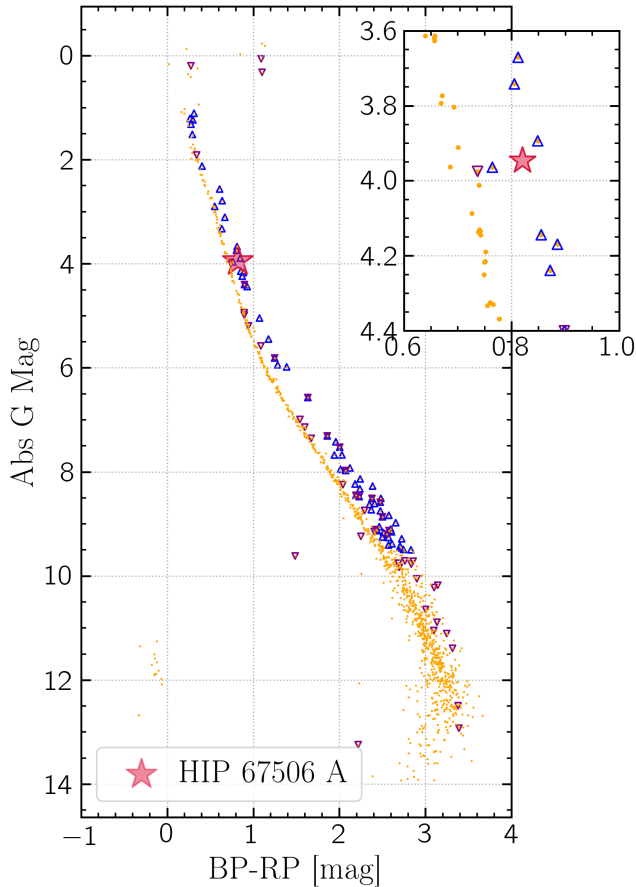


**Figure 2.** Gaia EDR3 BP minus RP vs absolute G magnitude color-magnitude diagram of Praesepe Cluster members identified in [Deacon & Kraus 2020](#) (orange). Objects they flagged as possible overluminous binaries are outlined in blue up-pointing triangles, and purple down-pointing triangles are objects they flagged with elevated astrometric noise, following their Figure 4. The position of HIP 67506 is marked with a red star in the main and inset axis, which shows a close view of the region surrounding HIP 67506 A. HIP 67506 A falls on the overluminous region above the main sequence, pointing to the presence of an unresolved stellar companion.

**Table 1.** Multiplicity Metrics for HIP 67506 A

Metric	Value
Gaia	
RUWE	2.02
astrometric_excess_noise	0.22
astrometric_excess_noise_sig	75.16
astrometric_chi2_al	2277.97
ipd_gof_harmonic_amplitude	0.0099
ipd_frac_multi_peak	0
Hipparcos-Gaia Accelerations	
HGCA $\chi^2$ ( <a href="#">Brandt 2021</a> )	41
$M_2$ at 23AU from from PMa ( <a href="#">Kervella et al. 2022</a> )	270 $M_{\text{Jup}}$

**Table 2.** Stellar Properties of HIP 67506 A

Parameter	Previous Value	Ref	Our Value
Distance (pc)	102±86	1	221.6±1.8 <sup>a</sup>
Mass ( $M_{\odot}$ )	1.2±0.1	2	1.2±0.2
Spectral Type	G5	3	F8–G2
$T_{\text{eff}}$ (K)	6077 ± 150	4	6000±350
Luminosity ( $L_{\odot}$ )	0.37 ± 0.07	4	1.91 <sup>+0.28</sup> <sub>-0.32</sub>
Sloan $m_{g'}$	11.04±0.01	5	11.04±0.01
Sloan $m_{r'}$	10.66±0.01	5	10.67±0.01
Sloan $m_{i'}$	10.56±0.01	5	10.59±0.01
Sloan $m_{z'}$	10.50±0.01	5	10.55±0.01
Sloan g-r	0.38±0.02	5	0.37±0.02
Sloan r-i	0.11±0.02	5	0.09±0.02

(1) [van Leeuwen 2007](#), (2) [Chandler et al. 2016](#),  
 (3) [Spencer Jones & Jackson 1939](#), (4) [McDonald et al. 2012](#),  
 (5) [Zacharias et al. \(2012\)](#), <sup>a</sup>[Gaia EDR3 Gaia Collaboration et al. \(2021\)](#)

marginally resolved sources ( $\rho \sim 0.1\text{--}1.2''$ , separation larger than the resolution limit but smaller than the confusion limit, [Gaia Collaboration et al. 2021](#)) present in the images, however the astrometric noise parameters are large and significant, affirming the presence of subsystems. This points to a companion near or below the resolution limit of  $\approx 0.1''$ .

Finally, HIP 67506 A also shows significant acceleration between the Hipparcos and Gaia astrometric measurements. The Hipparcos-Gaia Catalog of Accelerations (HGCA; [Brandt 2021](#)) measures the change in proper motion between a star's Hipparcos and Gaia proper motion measurements, as well as the positional difference between the missions, divided by the  $\sim 24$  year time baseline, and quantifies the deviation from linear motion. This acceleration is called the proper motion anomaly (PMa). The HGCA shows a significant PMa for HIP 67506 A, with a  $\chi^2 = 41$  for the goodness of fit of a linear proper motion to the measured astrometry. This points to unresolved subsystems causing acceleration.

Additionally, [Kervella et al. 2022](#) produced a PMa catalog for Hipparcos-Gaia EDR3 which also shows significant acceleration for HIP 67506 A (S/N = 9.31). They used the measured tangential velocity anomaly to constrain the mass of the object causing acceleration (which is degenerate with separation; [Kervella et al. 2019](#)). Using a mass of 1.3  $M_{\odot}$  for HIP 67506 A, they estimate a companion of mass 180  $M_{\text{Jup}}$  at 10 au causing the observed acceleration of HIP 67506 A. Extrapolating this out to the 2015 projected separation of HIP 67506 C (48 AU), the acceleration would be caused by a  $\sim 400 M_{\text{Jup}}$  object. The position angle of the acceleration given in [Kervella et al. 2022](#) is  $96.6 \pm 3.8^\circ$  for the 2016.0 Gaia epoch, which agrees within uncertainty with the candidate signal position angle in 2015.4, as would be expected if the candidate signal were the cause of the observed acceleration.

Combined with the candidate signal in our 2015 MagAO observation, these other lines of evidence point to a strong chance of this being a genuine companion signal which merited follow-up for confirmation and characterization.

## 3 OBSERVATIONS AND ANALYSIS

### 3.1 Observations

We observed HIP 67506 A on April 18th, 2022 with the extreme adaptive optics instrument MagAO-X ([Males et al. 2022](#)) on the 6.5m Magellan Clay Telescope at Las Campanas Observatory. We

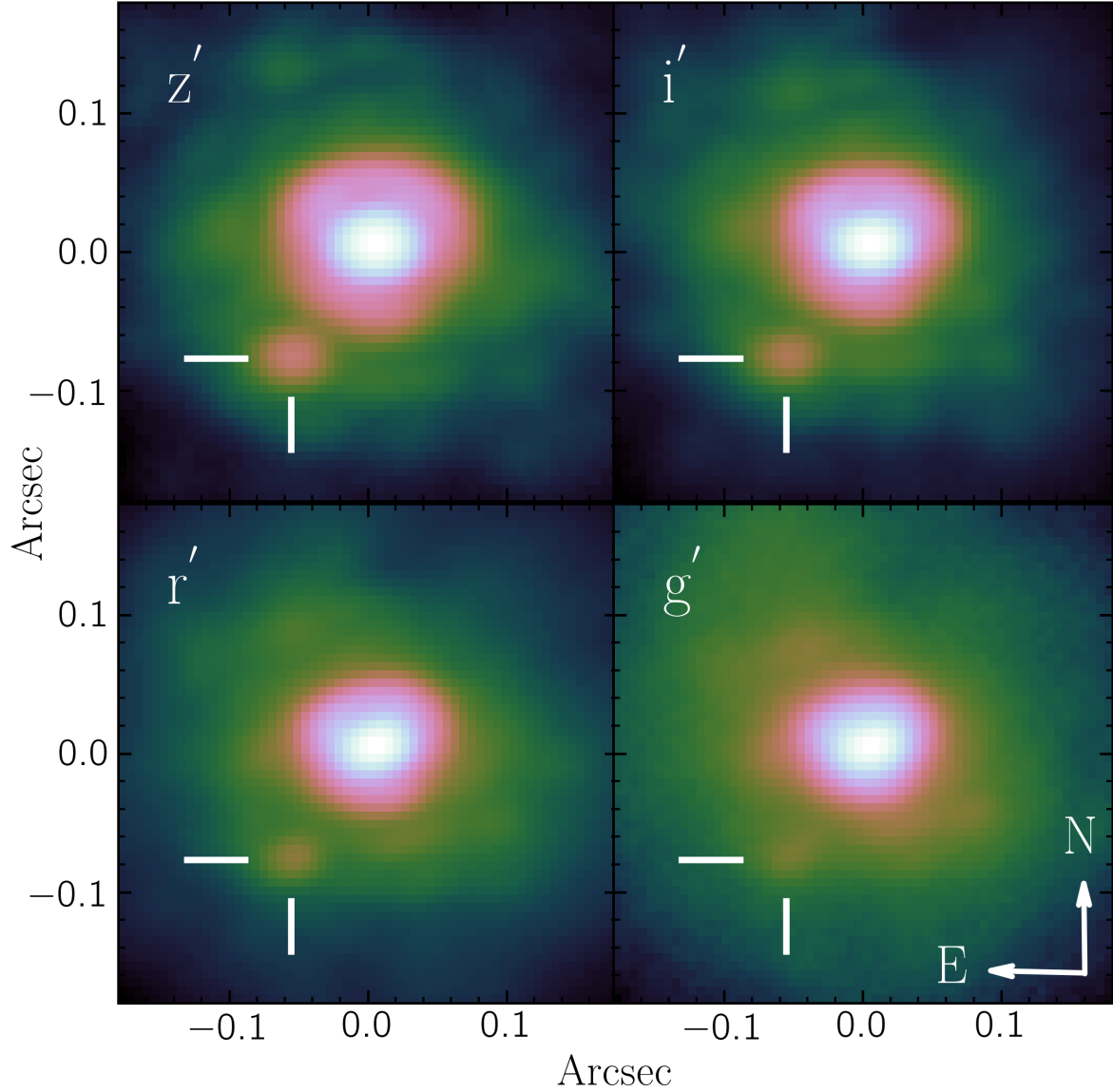


**Figure 3.** MagAO-X images of HIP 67506 A and HIP 67506 C in the four photometric filters  $g'$ ,  $r'$ ,  $i'$ ,  $z'$ , shown with log stretch. HIP 67506 A is centered in each image, and HIP 67506 C, located  $0.1''$  to the south east, is marked by the white pointers. North is up and East is left, and the stretch and spatial scale is same for each image.

observed HIP 67506 A in four science filters:  $g'$  ( $\lambda_0 = 0.527\mu\text{m}$ ,  $\Delta\lambda_{\text{eff}} = 0.044\mu\text{m}$ ),  $r'$  ( $\lambda_0 = 0.614\mu\text{m}$ ,  $\Delta\lambda_{\text{eff}} = 0.109\mu\text{m}$ ),  $i'$  ( $\lambda_0 = 0.762\mu\text{m}$ ,  $\Delta\lambda_{\text{eff}} = 0.126\mu\text{m}$ ), and  $z'$  ( $\lambda_0 = 0.908\mu\text{m}$ ,  $\Delta\lambda_{\text{eff}} = 0.130\mu\text{m}$ )<sup>3</sup>. MagAO-X is equipped with two science cameras, so we carried out science observations in two filters simultaneously. The science camera EMCCDs were set to 5 MHz readout speed with EM gain 100. Observations in  $r'$ ,  $i'$ , and  $z'$  had exposure time 0.115 sec;  $g'$  had exposure time of 3 sec. We obtained dark frames of the same settings. The pixel scale is  $6 \text{ mas pixel}^{-1}$  (Long et al. in prep), and the science and dark frames were  $512 \times 512$  pixels ( $3'' \times 3''$ ). Seeing was stable at  $0.4''$  throughout the observations.

We were unable to obtain observations of a photometric standard

star. We observed HIP 67121 as a photometric standard, only to discover that it is itself a binary with separation too close to resolve but large enough to distort the shape of the PSF core. We performed all further analysis using HIP 67506 A as a photometric reference.

To reduce the raw images in each filter, we dark subtracted each science frame, registered each frame using `PHOTUTILS DAOSTARFINDER` (Bradley et al. 2020; Stetson 1987) to find the peak of HIP 67506 A (uncertainty  $\pm 0.05$  pixels on peak finding) and `SCIPY NDIMAGE` (Virtanen et al. 2020) to center it, and rotated each frame to North up and East left (rotate CCW by telescope parallactic angle  $+ 1.995 \pm 0.61$  deg, Long et al. in prep). Finally we summed the images in each filter to maximize the signal to noise ratio of the faint companion.

Figure 3 displays the final images in each science filter, shown with a log stretch. The companion, HIP 67506 C, is clearly visible at

<sup>3</sup> Filter specifications and filter curves can be found in the MagAO-X instrument handbook at <https://magao-x.org/docs/handbook/index.html>



**Table 3.** Properties of HIP 67506 C

Parameter	Value
Stellar Properties	
Spectral Type	K7–M2
$T_{\text{eff}}$	$3600^{+250}_{-350}$ K
$\log(L)$	$-1.17^{+0.06}_{-0.08} L_{\odot}$
Sloan $m_{g'}$	$16.7 \pm 0.1$
Sloan $m_{r'}$	$15.61 \pm 0.05$
Sloan $m_{i'}$	$14.45 \pm 0.04$
Sloan $m_{z'}$	$14.05 \pm 0.03$
Sloan g-r	$1.1 \pm 0.1$
Sloan r-i	$1.16 \pm 0.07$
Astrometry	
2015-05-31	
Separation	$240 \pm 42$ mas
Position Angle	$85 \pm 13$ deg
2022-04-18	
Separation	$100.9 \pm 0.7$ mas
Position Angle	$145.1 \pm 0.8$ deg

0.1'' to the south east, indicated by the white cross-hairs. The spacial scale and stretch are the same in each image. The companion signal was strongest in the z' filter.

### 3.2 MagAO-X Photometry

*Measuring photometry.* We obtained relative photometry for each filter with the following procedure. We estimated the background level by computing the median value in a wide annulus far from the star's halo (0.6''–1.2''). We used PHOTUTILS aperture photometry tools to sum all pixels in an aperture of radius  $1.5\lambda/D$  centered on A, and subtracted the sum of pixels with the same aperture area valued at the background level, to estimate the flux from HIP 67506 A. To estimate the flux from HIP 67506 C we repeated the previous with an aperture of the same size centered at its location. We subtracted the mean background value from the image, computed a radial profile of the background subtracted image (excluding the region containing C), and used the flux at C's location in the radial profile to estimate the contribution from HIP 67506 A's halo at that location, and subtracted that as well. We converted the flux estimates into magnitudes and subtracted to obtain the contrast in MagAO-X filters.

*Uncertainty.* To estimate the uncertainty in the photometry measurements, we used the method of Mawet et al. 2014 for estimating signal to noise ratio in the regime of small number of photometric apertures, as we have at the separation of HIP 67506 C. At the separation HIP 67506 C, there are  $N = 2\pi r$  resolution elements of size  $\lambda/D$  (the characteristic scale of speckle noise), where  $r = n\lambda/D$  and  $n$  varies with the filter wavelength. We defined a ring of  $N-3$  resolution elements (neglecting those at and immediately to each side of HIP 67506 C) at separation  $r$  with radius  $0.5\lambda/D$ , then applied Eqn (9) of Mawet et al. (2014), which is the Student's two-sample t-test:

$$p(x, n2) = \frac{\bar{x}_1 - \bar{x}_2}{s_2 \sqrt{1 + \frac{1}{n_2}}} \quad (1)$$

where  $\bar{x}_1 = \text{HIP 67506 C flux}$ ,  $\bar{x}_2 = \text{mean}[\Sigma(\text{pixels in apertures})]$ ,  $s_2 = \text{stdev}[\Sigma(\text{pixels in apertures})]$ ,  $n_2 = N-3$ , and  $S/N = p$ . The

denominator of that equation is the noise term. We repeated this procedure for HIP 67506 A, defining a ring of apertures beyond the halo of both stars to estimate the background noise.

*Applying the standard.* We used HIP 67506 A as the photometric standard star, however literature photometry for HIP 67506 A consisted of a blend of flux from HIP 67506 A and HIP 67506 C, since it was previously unresolved. So to use HIP 67506 A as a standard we used our measured contrasts to separate the flux contributions from both stars. First we computed color transformations for MagAO-X filters to Sloan prime system filters using MagAO-X filter curves, public Sloan Digital Sky Survey transmission curves<sup>4</sup>, and a spectral type G5V model from the Pickles Atlas (Pickles 1998)<sup>5</sup>. We obtained published photometry for HIP 67506 A, displayed in Table 2, from the UCAC4 catalog (Zacharias et al. 2012) and converted to MagAO-X filters using our color transformation. We then computed the magnitude of HIP 67506 A and HIP 67506 C in the MagAO-X system as:

$$A_{\text{Flux}} + C_{\text{Flux}} = F_{0,\text{Vega}} \times 10^{-0.4 \times \text{Total mag in MagAO-X system}} \quad (2)$$

$$C_{\text{Flux}} = A_{\text{Flux}} \times \text{Flux Contrast} \quad (3)$$

$$A_{\text{Flux}} \times (1 + 10^{-0.4 \times \text{mag Contrast}}) = F_{0,\text{Vega}} \times 10^{-0.4 \times \text{Total mag}} \quad (4)$$

We then converted flux of A and C into the Sloan system using color transformation, displaying in Tables 2 and 3.

### 3.3 Astrometry

#### 3.3.1 Relative Astrometry Measurements

The 2015 MagAO/Clio L' epoch and 2022 MagAO-X epoch give relative astrometry spanning a 7 year baseline.

*The 2015 epoch.* The companion signal has been corrupted by the BDI KLIP algorithm – it is no longer a recognizable PSF shape, and in Pearce et al. 2022 we estimated a smaller flux than we measure in this work. The companion signal has been subject to over-subtraction by KLIP, and is not reliable for estimating photometry and astrometry (Soummer et al. 2012; Pueyo 2016).

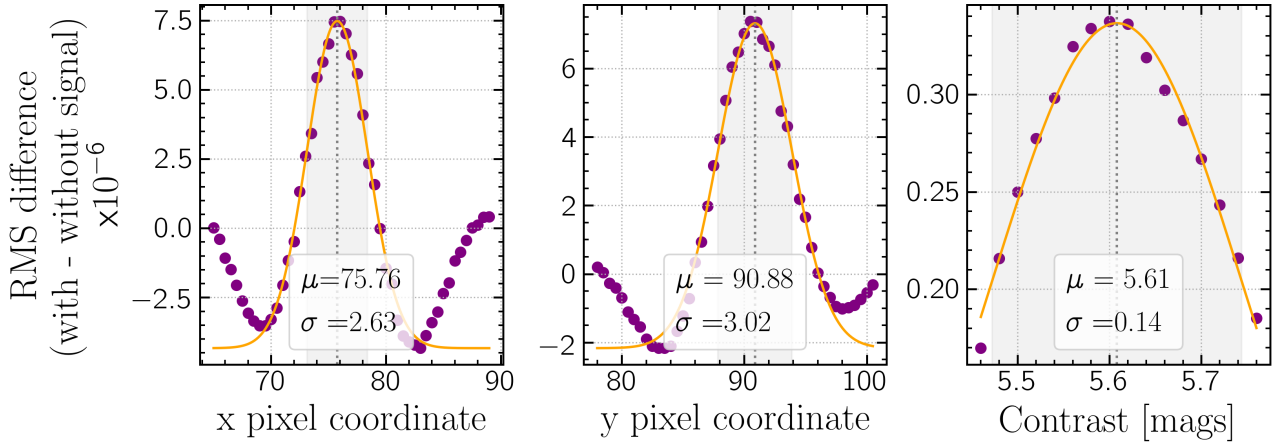
To estimate the position of the companion, we performed a grid search of the parameters which influence the signal strength in post-processing, similar to Morzinski et al. (2015) Appendix E. For a grid of  $[x, y]$  pixel position and contrast  $c$ , we injected a negative signal, modeled from the PSF of a median image of the HIP 67506 B 2015 dataset, into each HIP 67506 A image. We then performed KLIP reduction via the method in Pearce et al. 2022 and measured the root-mean-square (RMS) of pixels in a circle of radius  $1.5\lambda/D$  (~11 pixels) centered at the location of the companion signal.

Figure 4 displays the grid search results for the x-pixel coordinate (left), y-pixel coordinate (middle), and contrast (right) versus the difference in RMS between the reduced image with and without the injected signal. We fit a Gaussian to each parameter, while keeping the other parameters fixed at their best value, and took the mean and standard deviation as the best modeled parameter.

Figure 5 (top) shows the unsubtracted, KLIP-reduced image of HIP 67506 C (left, same as Figure 1, log stretch), the best value model

<sup>4</sup> <http://classic.sdss.org/dr3/instruments/imager/#filters>

<sup>5</sup> MagAO-X to SDSS color transformations for all spectral types can be found in the MagAO-X instrument handbook



**Figure 4.** Results of our grid search of  $[x, y, c]$  values for a model which minimizes HIP 67506 C residuals post-KLIP processing for the 2015 MagAO/Clio epoch. Each parameter is plotted versus the difference in RMS between KLIP-reduced image with and without the model subtracted. Each parameter was fit with a Gaussian function while keeping the others fixed at their peak value.

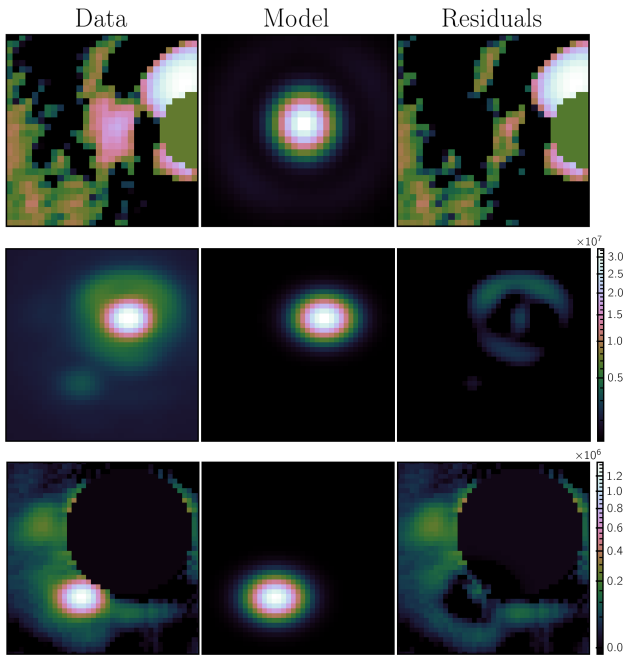


**Figure 5.** Top: Data, model, and residual of the  $[x, y, c]$  that minimizes residuals in 2015 MagAO/Clio observation. Data and residual images are post-KLIP processing, and shown with a log stretch; model image shows the signal with peak values in Figure 4 that was subtracted from images prior to KLIP processing. Middle and bottom: Data, model, and residuals from the 2D Gaussian model in the 2022 MagAO-X  $z'$  image for HIP 67506 A (middle) and HIP 67506 C (bottom).

from Figure 4 (middle, linear stretch), and the residuals post-KLIP with that model subtracted from each image pre-KLIP (right, log stretch). With HIP 67506 A registered at  $[x, y] = [89.5, 89.5]$  (origin is lower left), we find:  $\bar{x} = 75.76 \pm 2.63$  pixels, and relative separation  $\rho_x = 218 \pm 42$  mas;  $\bar{y} = 90.88 \pm 3.02$  pixels,  $\rho_y = -22 \pm 48$  mas; total separation and position angle is  $\rho = 240 \pm 42$  mas,  $\theta = 85 \pm 13$  deg.

*The 2022 epoch.* We measured the relative astrometry in the MagAO-X  $z'$  image following a modified version of the method de-

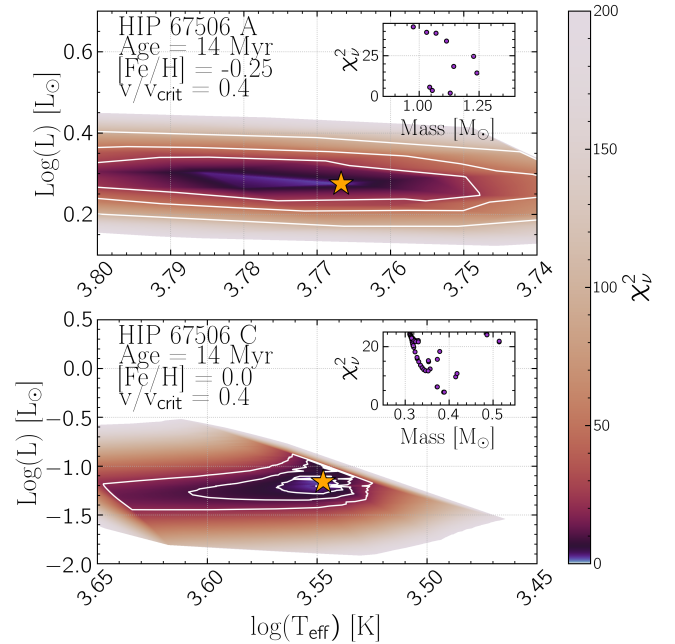


**Figure 6.** The lowest  $\chi^2$  of all MIST model fits occurred for age  $\sim 14$  Myr when ages were constrained to be the same for both objects. This figure shows the map of the reduced  $\chi^2$  surface in  $\log(T_{\text{eff}})$  and  $\log(L)$  for HIP 67506 A (top) and HIP 67506 C (bottom) for age = 14 Myr and the best-fitting values of metallicity and rotation for each. The lowest reduced  $\chi^2$  value for each is marked with an orange star. Contours denote  $\chi^2 = 25, 50$ , and 100. Inset axis:  $\chi^2$  of model versus model star mass for fits of models with age = 14 Myr. The lowest  $\chi^2$  values occurred at  $M_A = 1.13 M_{\odot}$  and  $M_C = 0.39 M_{\odot}$ .

scribed in Pearce et al. (2019) and Pearce et al. (2021). We modeled the PSF core as a simple 2-dimensional Gaussian function and varied the model parameters using the python Markov Chain Monte Carlo package EMCEE (Foreman-Mackey et al. 2013) with 100 walkers. Our model had seven parameters:  $x, y$  subpixel position (Gaussian prior with  $\mu =$  center from DAOSTarFinder,  $\sigma = \text{FWHM}/2.35$ ,  $\text{FWHM} = 1/\lambda D$  at  $z' = 0.03''$ ), amplitude (Gaussian prior with  $\mu =$  peak from DAOSTarFinder,  $\sigma =$  Poisson noise), background level (Gaussian prior with  $\mu =$  mean background level,  $\sigma =$  background

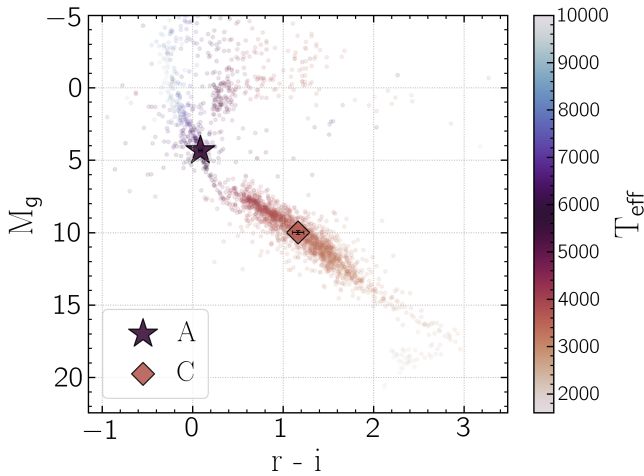


**Figure 7.** Color-magnitude diagram (CMD) of Sloan  $r'-i'$  vs. Sloan  $g'$  absolute magnitude. Points are photometry from the CARMENES sample of well-characterized M- and L dwarfs (Cifuentes et al. 2020) and a selection of Hipparcos stars with SDSS photometry and  $T_{\text{eff}}$  estimates from McDonald et al. 2012. Our photometry of HIP 67506 A (star) and HIP 67506 C (diamond) and uncertainties (black errorbars) are overplotted. A and C are colored according to the  $T_{\text{eff}}$  of the best-fit MIST model shown in Figure 6. The best-fitting MIST models correspond to  $T_{\text{eff}}$  values consistent with nearby objects on the CMD.

noise), Gaussian width in the  $x$  and  $y$  direction (Gaussian prior with  $\mu = \text{FWHM}/2.35$ ,  $\sigma = 0.01$ ), and rotation relative to  $x$  axis (Uniform prior on  $[0, \pi/2]$ ). The chains converged quickly and we found that 5000 steps was sufficient for chains to converge (Gelman-Rubin statistic  $< 1.2$  for all parameters), with a burn-in of 1000 steps.

We computed the model fit for the location of HIP 67506 A and HIP 67506 C in the 2022  $z'$  image, where HIP 67506 C's signal was strongest. The data, model, and residuals for the two measurements are shown in Figure 5 (middle and bottom). We used the MagAO-X astrometric solution (Long et al., in prep)<sup>6</sup> to compute  $[\rho \text{ (mas)}, \theta \text{ (deg)}]$  for each  $[\Delta x, \Delta y]$  (pixels) between A and C in the MCMC chains, then took the mean and standard deviation as the  $[\rho, \theta]$  for the 2022 epoch. Detector distortion is negligible at  $0.1''$  (Long et al. in prep). We find  $\rho = 100.9 \pm 0.7 \text{ mas}$ ,  $\theta = 145.1 \pm 0.8 \text{ deg}$ .

## 4 RESULTS

### 4.1 Photometry

We compared our magnitudes in the Sloan filter system with synthetic photometry from two stellar evolution grids, the Mesa Isochrones and Stellar Tracks (MIST, Dotter 2016; Choi et al. 2016; Paxton et al. 2011, 2013, 2015), and stellar tracks and isochrones with the Padova and Trieste Stellar Evolution Code (PARSEC, Bressan et al. 2012).

We used our absolute  $g'$ ,  $r'$ ,  $i'$ , and  $z'$  SDSS magnitudes for HIP 67506 A and HIP 67506 C as well as  $g'-r'$  and  $r'-i'$  colors for evaluating which models in each grid best describe our observations. For each isochrone set we minimized the  $\chi^2$  of the synthetic

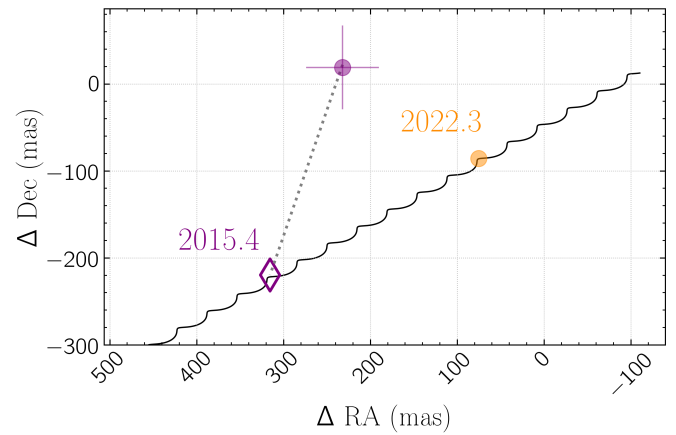


**Figure 8.** Relative astrometry of HIP 67506 C relative to A for the MagAO 2015 epoch (purple) and the MagAO-X 2022 epoch (orange). The abscissa and ordinate axes display position of HIP 67506 C relative to A in mas in right ascension (RA) and declination (Dec). The motion of a non-moving background object at the position of HIP 67506 C is given by the black track; the predicted position in 2022, given then 2015 position, is an open diamond. The observed position and uncertainty in each epoch is shown as filled circles (uncertainties are smaller than the marker for the 2022 epoch). The observed motion of the HIP 67506 C is not consistent with a background object, and is likely due to orbital motion.

photometry to our data as

$$\chi^2 = \sum \left( \frac{M_{x,\text{obs}} - M_{x,\text{model}}}{M_{x,\text{uncert}}} \right)^2 \quad (5)$$

where  $M_x$  is the absolute magnitude in a given filter or  $\Delta$  magnitude in a color. We imposed the constraint that the age must be the same for HIP 67506 A and HIP 67506 C, and computed the final goodness of fit as  $\chi^2 = \chi_A^2 + \chi_C^2$ .

We obtained the MIST<sup>7</sup> isochrone synthetic photometry in the SDSS  $ugriz$  system with rotation rate  $v/v_{\text{crit}} = 0.0$  and  $0.4$ ,  $[\text{Fe}/\text{H}] = [-4.00, -2.00]$  in  $0.50$  dex steps and  $[\text{Fe}/\text{H}] = [-2.00, +0.50]$  in  $0.25$  dex steps, and  $\log(\text{Age}) = [5.0, 10.3]$  in  $0.05$  dex steps.

For MIST isochrone  $\chi^2$  minimization, we determine  $T_{\text{eff}} = 6000 \pm 350 \text{ K}$  and  $\log(L) = 0.28^{+0.06}_{-0.08} L_{\odot}$  for HIP 67506 A,  $T_{\text{eff}} = 3600^{+250}_{-350} \text{ K}$  and  $\log(L) = -1.17^{+0.06}_{-0.08} L_{\odot}$  for HIP 67506 C.

Figure 6 shows the reduced  $\chi^2$  surface for  $\log(T_{\text{eff}})$  and  $\log(L)$  for the overall lowest  $\chi^2$  MIST isochrone ( $\chi^2 = 36.7$ ), with age = 14 Myr, rotation  $v/v_{\text{crit}} = 0.4$ , and  $[\text{Fe}/\text{H}] = 0.25$  for A and  $[\text{Fe}/\text{H}] = 0.0$  for C. Values of  $\log(T_{\text{eff}})$  are not well constrained for A, spanning from  $\log(T_{\text{eff}}) \sim 3.76\text{--}3.78$  (5700–6000K). The insets in Figure 6 display reduced  $\chi^2$  as a function of mass at  $M_A = 1.1M_{\odot}$ ,  $M_C = 0.4M_{\odot}$ . A second local minimum ( $\chi^2 = 39.2$ ) occurred at age = 5.6 Gyr,  $M_A = 1.1M_{\odot}$ , and  $M_C = 0.65M_{\odot}$ . (A plot of  $\chi^2_{\text{min}}$  as a function of age is included in the supplementary material.)

We used PARSEC version 1.2.5<sup>8</sup> with the YBC bolometric correction library (Chen et al. 2019) and revised Vega SED from Bohlin et al. (2020), and retrieved isochrone tables from  $\log(\text{age}) = [6.0, 10.13]$  dex in intervals of  $0.1$  dex and metallicities  $[\text{M}/\text{H}] = [-4.0, 0.5]$  dex in intervals of  $0.5$  dex, with synthetic photometry in the SDSS

<sup>6</sup> Available in the MagAO-X instrument handbook, <https://magao-x.org/docs/handbook/>

<sup>7</sup> Accessed from [https://waps.cfa.harvard.edu/MIST/model\\_grids.html](https://waps.cfa.harvard.edu/MIST/model_grids.html)

<sup>8</sup> Accessed from <http://stev.oapd.inaf.it/cgi-bin/cmd>

ugriz system. For PARSEC isochrone  $\chi^2$  minimization, we determine  $T_{\text{eff}} = 6000 \pm 350$  K and  $\log(L) = 0.29^{+0.06}_{-0.08} L_{\odot}$  for HIP 67506 A,  $T_{\text{eff}} = 3600^{+250}_{-350}$  K and  $\log(L) = -1.18^{+0.06}_{-0.08} L_{\odot}$  for HIP 67506 C. Our photometry was insufficient to place meaningful constraints on the age of either star.

Figure 7 shows a color-magnitude diagram of SDSS r-i color vs. SDSS g absolute magnitude. HIP 67506 A (purple star) and HIP 67506 C (orange diamond) are plotted with our photometry and colored according to our isochrone-derived  $T_{\text{eff}}$  estimates. Also plotted are reference stars from the CARMENES sample of well-characterized M- and L dwarfs (Cifuentes et al. 2020) and a selection of Hipparcos stars with SDSS photometry and  $T_{\text{eff}}$  estimates from McDonald et al. 2012. Our colors and temperature estimates are consistent with the reference stars. We estimate the spectral type of HIP 67506 A and HIP 67506 C to be  $\text{SpT}_A \approx \text{F8V-G2V}$  and  $\text{SpT}_C \approx \text{K7V-M2V}$ .

## 4.2 Astrometry

Figure 8 displays a common proper motion plot of HIP 67506 C relative to HIP 67506 A. We show the observed separation of HIP 67506 C in right ascension and declination for the 2015 and 2022 epochs (filled circles and error bars), the expected track if HIP 67506 C were a non-moving background object (zero proper motion; black track), and the predicted position of HIP 67506 C at the 2015 observation if it were a background object (open diamond). The observed position of HIP 67506 C does not follow the expected motion for a distant background object. We infer that the relative motion of HIP 67506 C is more consistent with a bound object than an unassociated object. This is supported by the large proper motion anomaly of HIP 67506 A.

Using the two position angles of Table 3, we determined that the position angle of HIP 67506 C at the Gaia epoch of 2016.0 was  $90 \pm 12^\circ$ , which agrees with the proper motion anomaly vector PA at the Gaia epoch of  $96.6 \pm 4.1^\circ$  (Kervella et al. 2022).

Our astrometry was insufficient to meaningfully constrain the orbit or dynamical mass, due to there being only two astrometric points and large error bars on the 2015 epoch.

## 5 CONCLUSION

We have shown that HIP 67506 A has a previously unknown  $0.1''$  companion, originally detected in 2015 with MagAO/Clio and BDI in  $L'$ . The shape was distorted from a typical PSF due to post-processing, and might have been easily dismissed with the other residuals at that radius. However several secondary indications hinted that the dubious candidate companion signal for HIP 67506 A in Pearce et al. (2022) was a strong candidate and merited follow-up observations: the poor Gaia astrometric signal, the significant PMA with the right acceleration vector angle, and the overluminosity of the Gaia photometry. Our analysis in Pearce et al. 2022 pointed to a possible high mass brown dwarf. We followed up in 2022 with MagAO-X and the companion was immediately and easily detected and determined to be a low mass star. The low S/N signal of HIP 67506 C at such a small IWA was bolstered by secondary indicators, which turned out to be powerful predictors of the genuine companion. We estimate HIP 67506 A and HIP 67506 C to be type F8–G2 and K7–M2 respectively. Further astrometric and photometric measurements are required to constrain properties and orbital elements.

## ACKNOWLEDGEMENTS

L.A.P. acknowledges research support from the NSF Graduate Research Fellowship. This material is based upon work supported by the National Science Foundation Graduate Research Fellowship Program under Grant No. DGE-1746060.

J.D.L. thanks the Heising-Simons Foundation (Grant #2020-1824) and NSF AST (#1625441, MagAO-X).

S.Y.H was supported by NASA through the NASA Hubble Fellowship grant #HST-HF2-51436.001-A awarded by the Space Telescope Science Institute, which is operated by the Association of Universities for Research in Astronomy, Incorporated, under NASA contract NAS5-26555.

MagAO-X was developed with support from the NSF MRI Award #1625441. The Phase II upgrade program is made possible by the generous support of the Heising-Simons Foundation.

We thank the LCO and Magellan staffs for their outstanding assistance throughout our commissioning runs.

This work has made use of data from the European Space Agency (ESA) mission *Gaia* (<https://www.cosmos.esa.int/gaia>), processed by the *Gaia* Data Processing and Analysis Consortium (DPAC, <https://www.cosmos.esa.int/web/gaia/dpac/consortium>). Funding for the DPAC has been provided by national institutions, in particular the institutions participating in the *Gaia* Multilateral Agreement.

This research has made use of the Washington Double Star Catalog maintained at the U.S. Naval Observatory.

*Facilities:* Las Campanas Observatory, Magellan:Clay (MagAO-X)

*Software:* Numpy (Harris et al. 2020), Astropy (Price-Whelan et al. 2018), Matplotlib (Hunter 2007), Scipy (Virtanen et al. 2020), emcee (Foreman-Mackey et al. 2013), corner.py (Foreman-Mackey 2016), Photutils (Bradley et al. 2020)

## DATA AVAILABILITY

The data underlying this article are available in at <https://github.com/logan-pearce/HIP67506-AC-Public-Data-Release> and at DOI: 10.5281/zenodo.7098006.

## REFERENCES

- Baraffe I., Homeier D., Allard F., Chabrier G., 2015, *A&A*, **577**, A42  
 Belokurov V., et al., 2020, *MNRAS*, **496**, 1922  
 Bohlin R. C., Hubeny I., Rauch T., 2020, *AJ*, **160**, 21  
 Bradley L., et al., 2020, astropy/photutils: 1.0.0, doi:10.5281/zenodo.4044744, <https://doi.org/10.5281/zenodo.4044744>  
 Brandt T. D., 2021, *ApJS*, **254**, 42  
 Bressan A., Marigo P., Girardi L., Salasnich B., Dal Cero C., Rubele S., Nanni A., 2012, *MNRAS*, **427**, 127  
 Bryan M. L., Knutson H. A., Lee E. J., Fulton B. J., Batygin K., Ngo H., Meshkat T., 2019, *AJ*, **157**, 52  
 Chandler C. O., McDonald I., Kane S. R., 2016, *AJ*, **151**, 59  
 Chen Y., et al., 2019, *A&A*, **632**, A105  
 Choi J., Dotter A., Conroy C., Cantiello M., Paxton B., Johnson B. D., 2016, *ApJ*, **823**, 102  
 Cifuentes C., et al., 2020, *A&A*, **642**, A115  
 Clarke C. J., 2020, *MNRAS*, **491**, L72  
 Close L. M., et al., 2013, *The Astrophysical Journal*, **774**, 94  
 Cutri R. M., et al., 2003, VizieR Online Data Catalog, p. II/246



Cutri R. M., et al., 2012, Explanatory Supplement to the WISE All-Sky Data Release Products, Explanatory Supplement to the WISE All-Sky Data Release Products

Deacon N. R., Kraus A. L., 2020, arXiv:2006.06679 [astro-ph]

Dotter A., 2016, *ApJS*, **222**, 8

ESA., 1997, VizieR Online Data Catalog, p. I/239

Fabricsius C., Høg E., Makarov V. V., Mason B. D., Wycoff G. L., Urban S. E., 2002, *A&A*, **384**, 180

Foreman-Mackey D., 2016, *The Journal of Open Source Software*, 1

Foreman-Mackey D., Hogg D. W., Lang D., Goodman J., 2013, *PASP*, **125**, 306

Gagné J., et al., 2018, *The Astrophysical Journal*, 856, 23

Gaia Collaboration et al., 2021, *A&A*, **649**, A1

Harris C. R., et al., 2020, *Nature*, 585, 357

Hartkopf W. I., Mason B. D., Finch C. T., Zacharias N., Wycoff G. L., Hsu D., 2013, *AJ*, **146**, 76

Herman M. K., Zhu W., Wu Y., 2019, *AJ*, **157**, 248

Hunter J. D., 2007, *Computing In Science & Engineering*, 9, 90

Kervella P., Arenou F., Mignard F., Thévenin F., 2019, *A&A*, **623**, A72

Kervella P., Arenou F., Thévenin F., 2022, *A&A*, **657**, A7

Knapp W., Nanson J., 2018, *Journal of Double Star Observations*, **14**, 503

Lindgren L., 2018, Re-normalising the astrometric chi-square in Gaia DR2, [http://www.rssd.esa.int/doc\\_fetch.php?id=3757412](http://www.rssd.esa.int/doc_fetch.php?id=3757412)

Males J. R., et al., 2022, in Schreiber L., Schmidt D., Vernet E., eds, Society of Photo-Optical Instrumentation Engineers (SPIE) Conference Series Vol. 12185, Adaptive Optics Systems VIII. p. 1218509 (arXiv:2208.07299), doi:10.1117/12.2630584

Mason B. D., Wycoff G. L., Hartkopf W. I., Douglass G. G., Worley C. E., 2001, *AJ*, **122**, 3466

Mawet D., et al., 2012, in Clampin M. C., Fazio G. G., MacEwen H. A., Oschmann Jacobus M. J., eds, Society of Photo-Optical Instrumentation Engineers (SPIE) Conference Series Vol. 8442, Space Telescopes and Instrumentation 2012: Optical, Infrared, and Millimeter Wave. p. 844204 (arXiv:1207.5481), doi:10.1117/12.927245

Mawet D., et al., 2014, *The Astrophysical Journal*, 792, 97

McDonald I., Zijlstra A. A., Boyer M. L., 2012, *Monthly Notices of the Royal Astronomical Society*, 427, 343

Morzinski K. M., et al., 2015, *The Astrophysical Journal*, 815, 108

Nielsen E. L., et al., 2019, *The Astronomical Journal*, 158, 13

Paxton B., Bildsten L., Dotter A., Herwig F., Lesaffre P., Timmes F., 2011, *ApJS*, **192**, 3

Paxton B., et al., 2013, *ApJS*, **208**, 4

Paxton B., et al., 2015, *ApJS*, **220**, 15

Pearce L. A., Kraus A. L., Dupuy T. J., Ireland M. J., Rizzuto A. C., Bowler B. P., Birchall E. K., Wallace A. L., 2019, *The Astronomical Journal*, 157, 71

Pearce L. A., Kraus A. L., Dupuy T. J., Mann A. W., Huber D., 2021, *ApJ*, 909, 216

Pearce L. A., Males J. R., Weinberger A. J., Long J. D., Morzinski K. M., Close L. M., Hinz P. M., 2022, *MNRAS*, **515**, 4487

Pickles A. J., 1998, *PASP*, **110**, 863

Poleski R., et al., 2021, *Acta Astron.*, **71**, 1

Price-Whelan A. M., et al., 2018, *aj*, **156**, 123

Pueyo L., 2016, *ApJ*, **824**, 117

Rodigas T. J., Weinberger A., Mamajek E. E., Males J. R., Close L. M., Morzinski K., Hinz P. M., Kaib N., 2015, *The Astrophysical Journal*, 811, 157

Soummer R., Pueyo L., Larkin J., 2012, *The Astrophysical Journal Letters*, 755, L28

Spencer Jones H., Jackson J., 1939, Catalogue of 20554 faint stars in the Cape Astrogaphic Zone -40 deg. to -52 deg. For the equinox of 1900.0 giving positions, precessions, proper motions and photographic magnitudes. Her Majesty's Stationary Office (HMSO)

Stetson P. B., 1987, *PASP*, **99**, 191

Vigan A., et al., 2021, *A&A*, **651**, A72

Virtanen P., et al., 2020, *Nature Methods*, **17**, 261

Zacharias N., Finch C. T., Girard T. M., Henden A., Bartlett J. L., Monet D. G., Zacharias M. I., 2012, VizieR Online Data Catalog, p. I/322A

van Leeuwen F., 2007, *A&A*, **474**, 653

## APPENDIX A: HIP 67506 B IS NOT A WIDE BINARY COMPANION TO HIP 67506 A

The Gaia solutions for HIP 67506 A and HIP 67506 B show differing parallax solutions (A: source id = 6109011780753115776,  $\pi = 4.51$  mas; B: source id = 6109011742094383744,  $\pi = 0.55$  mas), indicating that HIP 67506 B is an order of magnitude more distant than HIP 67506 A. This raises the question if the two stars are actually a gravitationally bound pair versus a chance alignment of unassociated stars at different distances. We queried the Gaia catalog for all objects within a  $1^\circ$  radius of HIP 67506 A and used a simple Monte Carlo simulation to determine that, given the density of objects in the local region, the probability of a chance alignment of two stars within a  $9''$  radius is  $38.9 \pm 1.6\%$ . The probability of chance alignment of two stars within  $9''$  and 2 magnitudes is  $4.5 \pm 0.7\%$ . So it is plausible that they are a chance alignment.

The Washington Double Star Catalog (WDS; Mason et al. 2001) astrometry for this system (WDS J13500-4303 A and B) is shown in Table A1. Figure A1 displays the motion of HIP 67506 B relative to HIP 67506 A as observed in WDS (circles), the predicted position of HIP 67506 B if it were an unmoving background star and HIP 67506 A moved with the proper motion given by Gaia DR3 (black track and diamonds), and the Gaia DR3 proper motion and parallax track for HIP 67506 B (blue track). The WDS astrometry is consistent with the Gaia proper motion and parallax and not a gravitationally bound pair with common proper motion, indicating that the small parallax in Gaia DR3 for HIP 67506 B is correct and the two are unassociated.

Assuming a mass of  $1.2 M_\odot$  for both stars (since HIP 67506 B appears to have a similar brightness as A), the escape velocity at the current separation is  $1.306 \pm 0.005 \text{ km s}^{-1}$ . Taking the case of a face-on orbit (radial velocity =  $0 \text{ km s}^{-1}$ , the smallest possible value for the relative velocity vector), the observed linear motion shown in Figure A1 gives a velocity of  $24 \pm 2 \text{ km s}^{-1}$ , roughly  $14\sigma$  larger than the escape velocity. Clarke (2020) and Belokurov et al. (2020) showed that unresolved hierarchical triples and high RUWE astrometric solutions can produce relative velocities exceeding escape velocity and an apparent deviation from Newtonian gravity in the case of bound systems, so we are unable to entirely rule out their being a gravitationally bound system. But the remarkable agreement of WDS astrometry with the Gaia proper motion solutions strongly favors the Gaia parallaxes and proper motions being accurate.

We conclude that the two sources are not a gravitationally bound system, and that the star HIP 67506 B is not in fact a companion to HIP 67506 A, but a much further distant background star.

This paper has been typeset from a  $\text{\TeX}/\text{\LaTeX}$  file prepared by the author.

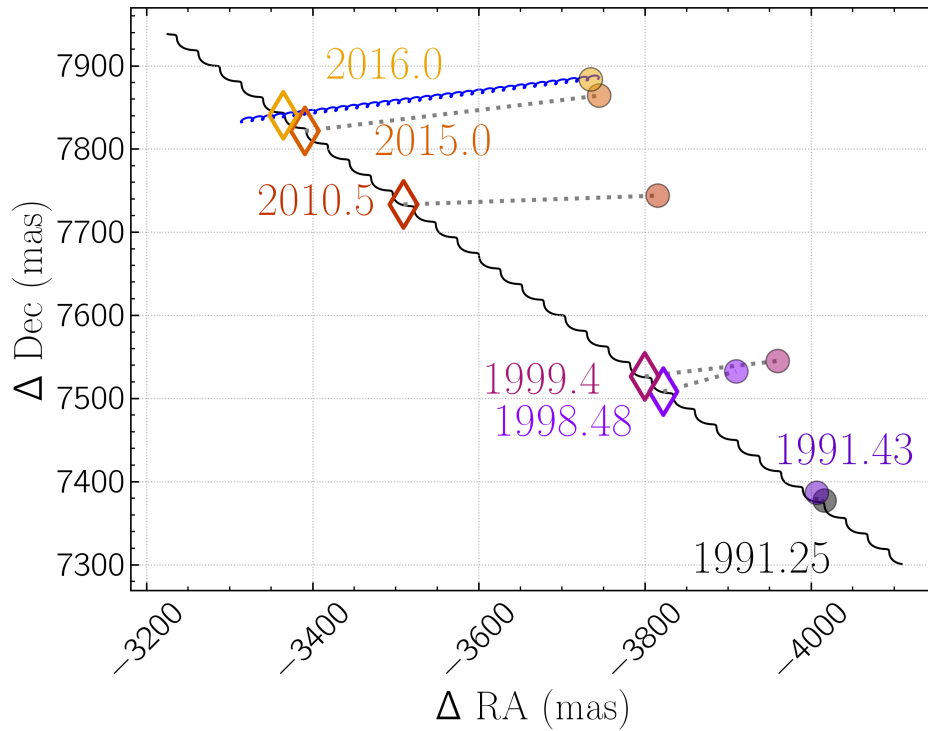


**Figure A1.** Relative astrometry of HIP 67506 A and HIP 67506 B (WDS J13500-4303 A and B). The abscissa and ordinate axes display position of HIP 67506 B relative to HIP 67506 A in mas in right ascension (RA) and declination (Dec). The motion of a non-moving background object at the position of HIP 67506 B is shown by the black track for the Gaia DR3 proper motion and parallax given for HIP 67506 B, with the predicted position at WDS observation epochs marked by colored diamonds. The blue track shows the track over the same time span given by the Gaia DR3 proper motion and parallax of HIP 67506 B. The observed WDS positions shown in Table A1 are marked by filled circles with corresponding epoch colors. The observed motion of HIP 67506 B relative to HIP 67506 A is consistent with the Gaia DR3 proper motion and not with a common proper motion pair. We conclude that the order-of-magnitude higher distance for HIP 67506 B than HIP 67506 A given by Gaia DR3 is correct.

**Table A1.** WDS catalog entry for HIP 67506 A and HIP 67506 B (WDS J13500-4303 A and B)

Date	Position Angle (deg)	PA Error (deg)	Sep (arcsec)	Sep Error (arcsec)	Ref
1991.25	323.3	-	9.190	-	ESA 1997
1991.43	323.4	-	9.19	-	Fabricius et al. 2002
1998.482	324.6	0.1	9.230	0.001	Hartkopf et al. 2013
1999.40	324.3	-	9.28	-	Cutri et al. 2003
2010.5	326.0	0.9	9.33	0.15	Cutri et al. 2012
2015.0	326.899	-	9.377	-	Knapp & Nanson 2018
2016.0	327.0363	0.0002	9.38593	3e-05	Gaia Collaboration et al. 2021